International Journal of Electrical, Electronic and Communication Sciences
ISSN: 2517-9438
Vol:9, No:4, 2015

Three Phase PWM Inverter for Low Rating Energy Efficient Systems

Nelson K. Lujara

***Abstract*—**The paper presents a practical three-phase PWM inverter suitable for low voltage, low rating energy efficient systems. The work in the paper is conducted with the view to establishing the significance of the loss contribution from the PWM inverter in the determination of the complete losses of a photovoltaic (PV) array-powered induction motor drive water pumping system. Losses investigated include; conduction and switching loss of the devices and gate drive losses. It is found that the PWM inverter operates at a reasonable variable efficiency that does not fall below 92% depending on the load. The results between the simulated and experimental results for the system with or without a maximum power tracker (MPT) compares very well, within an acceptable range of 2% margin**.**

***Keywords*—**Energy, Inverter, Losses, Photovoltaic.

I. Introduction

WITH continuous decline in prices of photovoltaic modules and other renewable energy sources in the international market, the design, cost and reliability of supplementary equipment such as dc-ac converters become increasingly important. Much work have been done on the optimization of the inverter as a part of a photovoltaic grid-connected system [1], study of dc-ac inverter suitable for both stand alone and grid connected photovoltaic systems [2] and problems associated with photovoltaic grid connected systems such as reactive power, harmonic contents and power factor [3], [4]. An appreciable number of works [5]-[9] discussing photovoltaic systems based on ac motor drive have been assuming an inverter to be a loss less device. In this paper, an analysis has been conducted with the view to establishing the significance of the loss characteristics of these inverters in the determination of overall losses of the system.

Photovoltaic systems based on inverter-fed induction motors have been proposed [1], [5], [6], [10], [11]. Induction motors are rugged, physically small compared to dc motors of the same power rating, cheap and require little maintenance. The disadvantages associated with this system is firstly, the cost of the dc-ac converter and secondly, the reduction of the system efficiency due to the inclusion of the converter in the system. For this reason, the overall efficiency of an induction motor-based drive system supplied by a PV array may be lower than that of the same system using a dc motor. Though the cost of an induction motor is less than say, a permanent magnet dc motor of the same rating, the cost involved in a complete converter unit continues to make the system expensive.

N. K. Lujara is with the Department of Electrical Engineering, College of Engineering and Technology, University of Dar es Salaam, P.O.Box 35131, Tanzania (phone: +255 754 554 403, e-mail: nklujara@gmail.com).

II. Circuit Description

Due to low efficiency of solar cells, high efficiency is a critical design requirement for any sub-system intended for photovoltaic applications. For the inverter, losses are primarily in the power semiconductor devices. Devices with controlled turn-off capability, such as transistors, MOSFET's, GTO's and IGBT's are commonly used depending on the required voltage and current ratings of the inverter. In this work, the inverter of Fig. 1, which uses MOSFET's as switching devices, is considered. The inverter supplies an induction motor driving a rotary pump for water pumping. The total inverter losses are calculated at various pumping heads, with the input power of the inverter obtained from the V-I characteristic of the PV array at an insolation of 1000 W/m^2 thus giving the power output and efficiency of the inverter. The experimental efficiency at various heads is obtained by measuring the output power of the inverter.

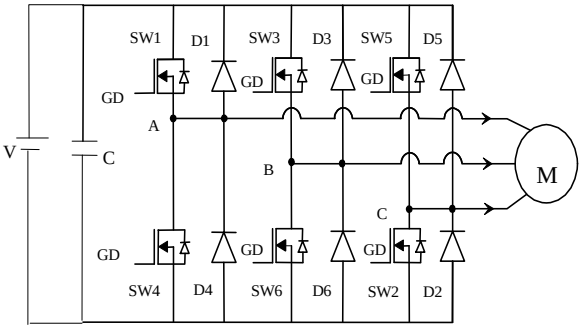

Fig. 1 Voltage source inverter feeding a three-phase induction motor (GD = gate drive, All switches: IRF 840, All freewheeling diodes: BYW29-200)

III. Analysis and Calculation of Inverter Efficiency

A. Analysis of Device Currents in a PWM Inverter

The waveform model upon which the analysis is based is shown in Fig. 2. The voltage waveform, which is drawn with a low frequency ratio for clarity, is the PWM pattern for one leg of the inverter shown in Fig. 1. The assumption made here is that the load current is sinusoidal and is given by;

$$i_l(t) = I_m \sin(\omega t - \theta_f) \quad (1)$$

where; I_m = peak value of the load current; θ_f = phase displacement between the load current and the voltage at fundamental frequency.

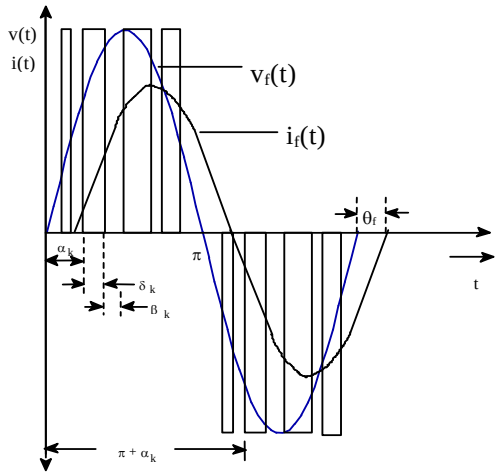

Fig. 2 The output current and voltage waveforms of PWM inverter

The number of pulses, p which is equal to the number of notches, q in one half cycle are determined from;

$$p = \frac{f_c}{2 f_o} \tag{2}$$

where; f_c = Carrier frequency; f_o = Modulating frequency.

In order to determine the width of the pulses and the notches, a triangular carrier wave sampling signal is compared directly with a sinusoidal modulating wave to determine the switching instants, and therefore the resultant pulse widths. A regular sampled PWM inverter control [12] of Fig. 3 is used, since in this type of control the sampling positions and sampled values are easily defined, such that the pulses produced are predictable both in width and position. The widths of the pulses, δ_k in Fig. 3 are defined by;

$$\delta_k = \frac{T}{2}\left[1 + M \sin \omega T_1\right] \tag{3}$$

and the width of the notches β_k are defined by;

$$\beta_k = \frac{T}{2}\left[1 + M \sin \omega T_2\right] \tag{4}$$

where; T = sampling interval; T_1, T_2 = sampling instants; M = modulating index; ω = angular frequency.

In order to determine the current in the devices (switch and freewheeling diode), the current due to each pair of voltage pulses and notches are calculated and then the effect of all pulses and notches are combined to obtain the effective currents.

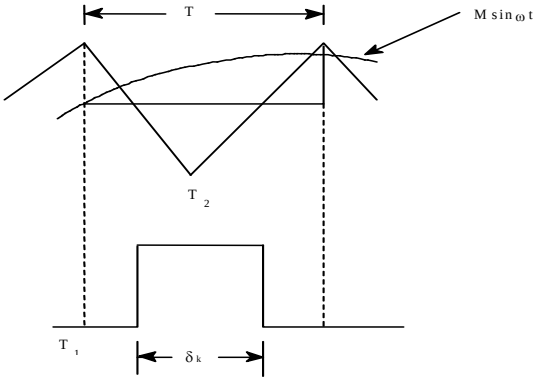

Fig. 3 Determination of pulse and notch width in a regular switching strategy PWM inverter

The k^{th} positive pulse is assumed to start at $\omega t = \alpha_k$ (Fig. 2) and the negative one of the same width starts at $\omega t = \pi + \alpha_k$. The k^{th} notch will start *at* $\omega t = \alpha_k + \delta_k$ and the negative notch of the same width will start at $\omega t = \pi + \alpha_k + \delta_k$.

The rms and average current in the switch are obtained using (5) and (6), respectively;

$$I_{srms} = \sqrt{\frac{1}{T} \cdot \sum_{k=1}^{p} \int_{\alpha_k}^{\alpha_k + \delta_k} \left(I_m \sin\left(\omega t - \phi_f\right)\right)^2 d\omega t} \tag{5}$$

$$I_{sav} = \frac{1}{T} \cdot \sum_{k=1}^{p} \int_{\alpha_k}^{\alpha_k + \delta_k} I_m \sin\left(\omega t - \phi_f\right) d\omega t \tag{6}$$

where; I_{srms} = rms current in the switch; I_{sav} = average current in the switch; α_k = the beginning of the k^{th} pulse; δ_k = the width of the k^{th} pulse.

The rms and average currents in the freewheeling diode are obtained using (7) and (8), respectively;

$$I_{frms} = \sqrt{\frac{1}{T} \cdot \sum_{k=1}^{p} \int_{\alpha_k + \delta_k}^{\alpha_k + \delta_k + \beta_k} \left(I_m \sin\left(\omega t - \varphi_f\right)\right)^2 d\omega t} \tag{7}$$

$$I_{fav} = \frac{1}{T} \cdot \sum_{k=1}^{p} \int_{\alpha_k + \beta_k}^{\alpha_k + \delta_k + \beta_k} I_m \sin\left(\omega t - \phi_f\right) d\omega t \tag{8}$$

B. Conduction Losses in the MOSFET

Conduction losses in one MOSFET of the inverter are determined as shown in (9):

$$P_c = I_{rms}^{\ 2} \cdot R_{DS(on)} \tag{9}$$

where; I_{rms} = rms current flowing in the switch; $R_{DS(ON)}$ = drain-to-source resistance at a junction temperature.

The switch rms current is obtained from (5). The total losses in the inverter are obtained by multiplying the losses in one switch with the number of switches in the inverter.

C. MOSFET Switching Losses

The switching losses are generally obtained from the following equation;

$$P_s = f_s \cdot \int_0^{t_s} v(t) \cdot i(t) dt \quad (10)$$

where; $f_s =$ switching frequency; $t_s =$ switching time; $v(t) =$ time dependent voltage in the switch; $i(t) =$ time dependent current in the switch.

In order to estimate the switching losses in the inverter, one leg of a three phase PWM inverter is considered as shown in Fig. 4. At the beginning of every switching cycle the load current is circulating through the freewheeling diode of one MOSFET prior to the turn-ON of the other.

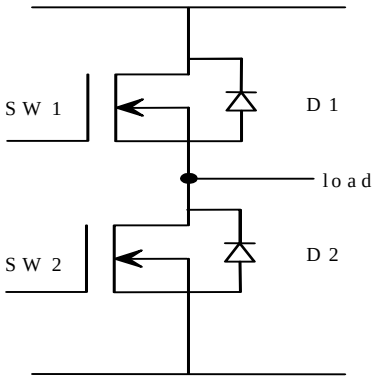

Fig. 4 One leg of a PWM inverter

The load current in one leg of the PWM inverter is shown in Fig. 5, with the upper switch and the bottom freewheeling diode conducting during the positive half cycle. The bottom switch and the top freewheeling diode conduct during the negative half cycle of the load current.

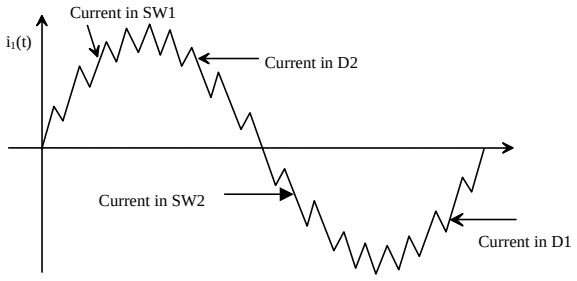

Fig. 5 The load current in one leg of a PWM inverter

The current waveform of the top switch (SW1) is shown in Fig. 6. The current is a series of pulses during the positive cycle of the load current. Fig. 7 shows one pulse of Fig. 6 expanded to show the turn-ON, conduction and turn-OFF portion of the switch. The voltage across the top switch is shown in Fig. 8.

The current pulse of Fig. 7 and one voltage pulse of Fig. 8 are expanded to show the approximate current turn-ON and OFF transients of the switch in Fig. 9. It is assumed that there is no stray inductance in the inverter circuits and hence no overvoltages during the switch turn-OFF characteristic.

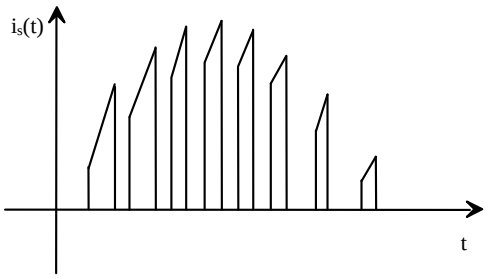

Fig. 6 The current waveforms of the top switch for one half cycle

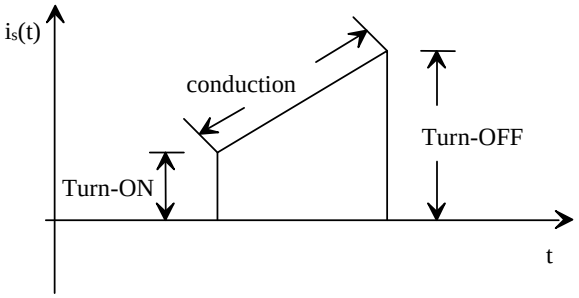

Fig. 7 The current waveforms of the top switch for one pulse

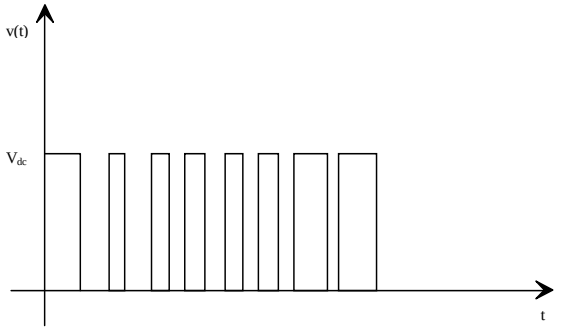

Fig. 8 The voltage across the top switch

1) Determination of Switching Losses in One Pulse of a PWM Inverter

The switching losses are calculated by first determining the losses in one pulse of Fig. 6 and then summing-up the effect of all pulses. The switch conduction current is different for each pulse. The loss in one pulse can be found if the switching instant, the pulse and notch widths are known.

The intersection of the peak point of the carrier frequency and the modulating signal (Fig. 3) for the k^{th} pulse, m_k is determined using (11);

$$m_k = \frac{\pi}{p} + T(k-1) \quad \text{k = 1, 2….p} \quad (11)$$

where;

$$T = \frac{\pi}{p}$$

The switching instant for the k^{th} pulse, α_k is determined from;

$$\alpha_k = \frac{\pi}{p} + T(k-1) - \left(\frac{T+\delta_k}{2}\right) \quad (12)$$

The conduction current through the switch during the k^{th} pulse, is obtained by substituting the k^{th} pulse switching instant α_k in (1) to obtain;

$$I_k = I_m \sin(\alpha_k - \theta_f) \quad \alpha_k > \theta_f \quad (13)$$

In order to evaluate switching losses, the approximate switching transient of Fig. 9 is first developed with the following assumptions:

(i) The switch current during one pulse is constant
(ii) The switch current is perfectly in phase with the fundamental component of current

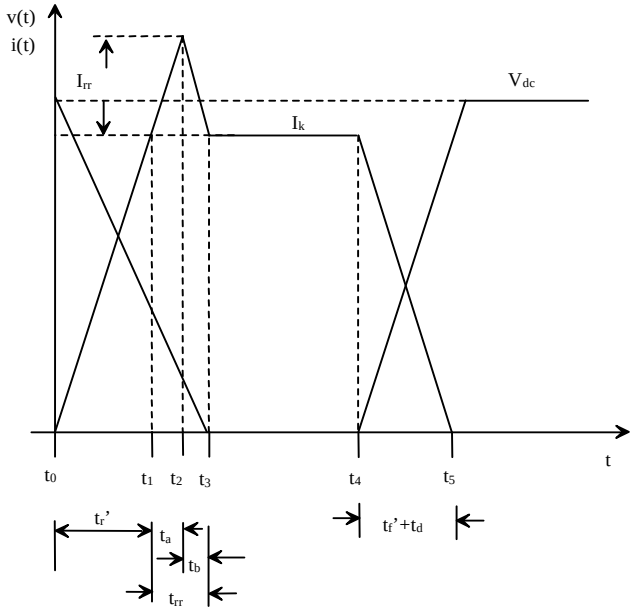

Fig. 9 Approximate turn-ON and OFF transients of a MOSFET in the PWM inverter

2) Turn-ON losses

From time t_0 *up to* t_1 (t_r'), the drain current builds up to the value of the load current supporting the immediate falling drain voltage. The current in the k^{th} pulse during this time is given by;

$$i(t) = I_k \cdot \frac{t}{t_r'} \quad (14)$$

where; $t_r' = 1.25 \times t_r$, since t_r (current rise time of the switch) is defined from 10% to 90%.

The voltage across the switch is falling from V_{dc} to 0 in time $t_t = t_r' + t_{rr}$. The voltage equation during this period is obtained from;

$$V_{dc} - V_{dc} \cdot \frac{t}{t_t} \quad (15)$$

where; t_{rr} = reverse recovery time of the freewheeling diode; V_{dc} = dc link voltage.

The turn-ON losses for the k^{th} pulse during this period are evaluated using (16) as;

$$P_1 = \frac{f_s}{p} \cdot \int_0^{t_r'} \left[V_{dc} - V_{dc} \cdot \frac{t}{t_t}\right] \cdot \left[I_k \cdot \frac{t}{t_r'}\right] dt \quad (16)$$

The total loss due to all pulses during this period is obtained using (17);

$$P_{T1} = \frac{f_s}{p} \cdot \sum_{k=1}^{p} \left[V_{dc} - V_{dc} \cdot \frac{t}{t_t}\right] \cdot \left[I_k \cdot \frac{t}{t_r'}\right] dt \quad (17)$$

During the time interval t_1-t_2, the load current and the diode reverse recovery current are carried by the MOSFET while blocking the available voltage. This period (t_1-t_2=t_a) represents the first part of the diode recovery loss. This period begins when the current in the diode is zero and ends when all carriers stored in the diode junction have recombined and the diode starts to regain its blocking capability. Based on experimental results, $t_a = \frac{t_{rr}}{3}$ [13]. The current and voltage equations during this period (Fig. 9) are obtained through (14) and (18) respectively;

$$v(t) = V_{dc} - V_{dc} \cdot \frac{t}{t_t} \quad (18)$$

The total switching losses due to all pulses during this interval are calculated as;

$$P_{T2} = \frac{f_s}{p} \cdot \sum_{k=1}^{p} \int_{t_r'}^{t_{ra}} \left[V_{dc} - V_{dc} \cdot \frac{t}{t_t}\right] \cdot \left[I_k \cdot \frac{t}{t_r'}\right] dt \quad (19)$$

where;

$$t_{ra} = t_r' + \frac{t_{rr}}{3}$$

At t_2 in Fig. 9, the freewheeling diode regains its reverse blocking capability and the voltage across the switch fall to its ON-state value. The current in the switch falls to the load current at that time. This is the second part of the diode reverse recovery characteristic. This period is given by,

$t_b = \frac{2}{3} \cdot t_{rr}$ [14]. The current equation in this duration is obtained as follows:

Let I_k' be the current in the switch during the k^{th} pulse at t_2, it follows from Fig. 9 that;

$$I_k' = I_k \cdot \frac{t_{ra}}{t_r'} \tag{20}$$

Let;

$$I_k'' = I_k - I_k' \tag{21}$$

The current equation from t_2 to t_3, i.e. from 0 to t_b is given by;

$$i(t) = I_k'' \cdot \frac{t}{t_b} + I_k' \tag{22}$$

Since the voltage is falling linearly from 0 to t_t, at t_2 the voltage across the switch, V_{dc}' is obtained from;

$$V_{dc}' = V_{dc} - V_{dc} \cdot \frac{t_{ra}}{t_t} \tag{23}$$

where;

$$t_t = t_r' + t_{rr}$$

The equation of the voltage from t_2 to t_3 (i.e. from 0 to t_b) is obtained from;

$$v(t) = V_{dc}' - V_{dc}' \cdot \frac{t}{t_b} \tag{24}$$

The turn-ON losses for the k^{th} pulse during this period are calculated as;

$$P_3 = \frac{f_s}{p} \cdot \int_0^{t_b} \left[\left(V_{dc}' - V_{dc}' \cdot \frac{t}{t_b} \right) \cdot \left(I_k'' \cdot \frac{t}{t_b} + I_k' \right) \right] dt \tag{25}$$

The total loss in this period for all pulses is calculated from;

$$P_{T3} = \frac{f_s}{p} \cdot \sum_{k=1}^{p} \int_0^{t_b} \left[\left(V_{dc}' - V_{dc}' \cdot \frac{t}{t_b} \right) \cdot \left(I_k'' \cdot \frac{t}{t_b} + I_k' \right) \right] dt \tag{26}$$

The total turn-ON loss in one switch is obtained from;

$$P_{ON} = P_{T1} + P_{T2} + P_{T3} \tag{27}$$

3) Turn-OFF Losses

The turn-OFF losses in one pulse of the switch occur during the period

$$t_4 - t_5 = t_f' + t_d;$$

where; $t_f' = 1.25 \times t_f$, since t_f is defined from 90% to 10% of the current fall time; t_f = current fall time; t_d = current turn-OFF delay time.

The current equation for the k^{th} pulse during this period is;

$$i(t) = I_k - I_k \cdot \frac{t}{t_t} \tag{28}$$

where;

$$t_t = t_f' + t_d$$

The voltage equation is;

$$v(t) = V_{dc} \cdot \frac{t}{t_t} \tag{29}$$

The turn-OFF loss in the k^{th} pulse is;

$$P_{F1} = \frac{f_s}{p} \cdot \int_0^{t_t} \left[\left(V_{dc} \cdot \frac{t}{t_t} \right) \left(I_k - I_k \cdot \frac{t}{t_t} \right) \right] dt \tag{30}$$

The turn-OFF loss in one switch is obtained through (31);

$$P_{OF} = \frac{f_s}{p} \cdot \sum_{k=1}^{p} \int_0^{t_t} \left[\left(V_{dc} \cdot \frac{t}{t_t} \right) \cdot \left(I_k - I_k \cdot \frac{t}{t_t} \right) \right] dt \tag{31}$$

The total switching loss is finally determined from the sum of the Turn-ON and Turn-OFF losses and the number of switches, i.e.

$$P_{sw} = 6 \cdot \left(P_{ON} + P_{OF} \right) \tag{32}$$

D. Conduction Losses in the Freewheeling Diode

The power dissipated in the drift region during the ON-state period of the diode is neglected due to conductivity modulation of the region. The conduction losses in the freewheeling diode are thus calculated based on the diode average forward current as [13];

$$P_{cf} = V_{on} \cdot I_{fav} \tag{33}$$

where; V_{on} = ON-state voltage drop of the diode; I_{fav} = average current in the diode.

The diode average current is given by (8). The total diode conduction losses in the PWM inverter are obtained by multiplying the losses in one diode with the number of diodes in the inverter.

E. Switching Losses in the Freewheeling Diode

Switching losses in a freewheeling diode are classified as turn-ON and turn-OFF losses. The forward turn-ON time of the freewheeling diode that was used in the inverter is negligible [15] and this renders turn-ON losses of the diode negligible. Fig. 10 shows the approximate switching

characteristic of one pulse of the freewheeling diode in the PWM inverter. Turn-OFF losses (reverse recovery losses) are significant during the period t_b when the dc link voltage appears across the diode. During period t_a, turn-OFF losses are negligible since the voltage across the diode is the ON-voltage of the diode.

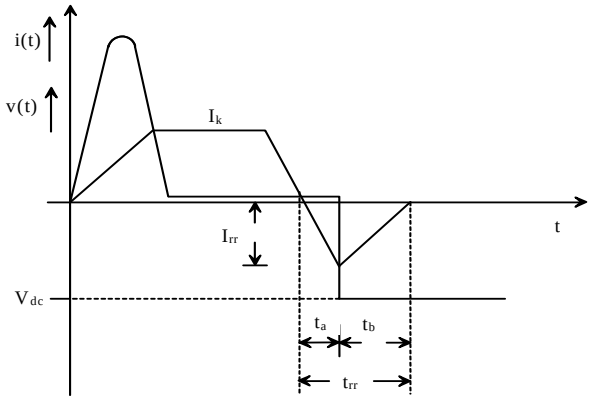

Fig. 10 Approximate switching transients of the freewheeling diode

F. Reverse Recovery Losses of the Freewheeling Diode

The current equation during the period t_b is given by;

$$i(t) = I_{rr} - I_{rr} \cdot \frac{t}{t_b} \tag{34}$$

where; I_{rr} = peak reverse current.

The duration, t_b is the time when the metallurgical junction of the diode is reverse biased. This time was established experimentally and was found to be approximately equal to $\frac{2}{3} \cdot t_{rr}$ [11].

The peak reverse current, I_{rk} of the diode for the k^{th} notch is established using the turn-ON transient of the switch (Fig. 9) as;

$$I_{rk} = I_k \cdot \frac{t_t}{t_r'} - I_k \tag{35}$$

The voltage across the diode during the period t_b is the dc-link voltage.

The reverse recovery losses for the k^{th} pulse are calculated through (36);

$$P_R = \frac{f_s}{p} \cdot \int_0^{t_b} \left(I_{rk} - I_{rk} \cdot \frac{t}{t_b} \right) \cdot V_{dc} \tag{36}$$

The total reverse recovery loss is the sum of losses in all pulses as given in (37);

$$P_{RT} = \frac{f_s}{p} \cdot \sum_{k=1}^{p} \int_0^{t_b} \left(I_{rk} - I_{rk} \cdot \frac{t}{t_b} \right) \cdot V_{dc} \tag{37}$$

G.Losses in the Gate Drive

The power output of the gate drive is determined during turn-ON and OFF of the MOSFET, when the gate capacitance is being charged or discharged. The charge stored in the gate capacitor is dependent on the gate-to-source voltage, V_{gs}. The power output is calculated using (38);

$$P_g = 2 \cdot Q_{gs} \cdot V_{gs} \cdot f_s \tag{38}$$

where; Q_{gs} = gate-to-source charge; f_s = switching frequency.

Gate drive losses, P_l are calculated from;

$$P_l = P_i - P_g \tag{39}$$

where; P_i = input power to the gate drive.

H.Inverter Efficiency

Inverter efficiency η_{inv} is obtained from;

$$\eta_{inv} = \frac{P_a - P_{inv}}{P_a} \tag{40}$$

where; P_a = inverter input power; P_{inv} = total inverter losses.

IV. Experimental Determination of Inverter Efficiency

A. Method of Measurements

Losses in the inverter were determined by measuring the output and input power to the inverter. The inverter input voltage and current at a given head at an insolation of 1000 W/m^2 were obtained from the V-I characteristic of the PV array. The output power of the inverter was measured using the ERICH MAREK voltage-current-power meter. This meter is a thermal instrument and therefore measures true rms voltage and current. It measures the non-sinusoidal voltage and current output waveforms of the inverter accurately. The meter is designed for a bandwidth from dc to 50 kHz with an accuracy of 0.5% and operates from a few milliwatts to 4 kW, with current ranges from 6 mA to 6 A and voltage ranges from 1.5 V to 600 V.

With the above measurements, the inverter efficiency, η_{inv} at various heads was determined using (41);

$$\eta_{inv} = \frac{P_o}{P_i} \tag{41}$$

where; P_i = array output power; P_o = inverter output power.

V. Experimental Results

Tables I and II show the simulated and experimental inverter efficiencies for the PV water pumping systems with and without maximum power tracker at a head of 15m-45m at

a constant insolation of 1000 W/m^2. The sinusoidal PWM inverter was operated at a switching carrier frequency of 5 kHz.

TABLE I
SIMULATED AND EXPERIMENTAL INVERTER EFFICIENCIES OF THE PV SYSTEM WITHOUT MPT

Head (metres)	Inverter efficiency Simulation (%)	Inverter efficiency Experimental (%)	% Error
15	95.87	94.4	1.53
20	95.44	94.1	1.4
25	95.06	93.8	1.26
30	94.78	93.4	1.38
35	94.02	92.8	1.22
40	93.69	92.5	1.19
45	93.28	92.1	1.18

TABLE II
SIMULATED AND EXPERIMENTAL INVERTER EFFICIENCIES OF THE PV SYSTEM WITH MPT

Head	Inverter efficiency Simulation (%)	Inverter efficiency Experimental (%)	% Error
15	96.01	94.9	1.16
20	95.84	94.6	1.29
25	95.52	94.1	1.49
30	95.08	93.7	1.45
35	94.78	93	1.88
40	94.36	92.8	1.65
45	94.16	92.2	2.1

$$\% \text{ Error} = \frac{\text{Simulation value} - \text{Measured value}}{\text{Simulated value}} \times 100\,\%$$

VI. DISCUSSION OF RESULTS

Based on the results presented in Tables I and II, the simulated and the measured efficiencies at an insolation of 1000 W/m^2 for the system with and without MPT compares very well, with the simulated values higher than the measured values within a 2% error margin. The source of errors is mainly attributed to limitation in the accuracy of the measuring instruments and the exclusion of the inverter harmonics in the simulation model.

VII. CONCLUSIONS

The following conclusions are made regarding this work;

1) For low power applications, MOSFET based PWM inverters have sufficient but not negligible efficiency for photovoltaic applications
2) The losses in the inverter can be reasonably estimated using information from data sheets

REFERENCES

[1] R. Pickrell, G. O'Sullivan, W. Merrill, "An inverter/controller subsystem optimized for photovoltaic applications" Proc. 13th IEEE Photovoltaic Specialist Conference, IEEE, New York, 1978, pp 984-991
[2] L. Bonte, D. Baert, "A low distortion PWM power conditioning system for line coupled and stand alone residential photovoltaic applications" 5th European Community Photovoltaic Solar Energy Conference, Athens, Greece, 1983, pp 545-549
[3] Li Fen et al, " A novel model for daily energy production restriction of grid-connected photovoltaic system" Journal of Solar Energy Engineering, Vol. 138, Issue 3, 2015
[4] P. Longrigg, "DC to AC inverters for photovoltaics" Solar cells 6 (1982) pp 343-356
[5] R. Sridhar, "Investigation on a modified 11-level cascaded inverter fed by photovoltaic array stand-alone applications" Journal of Solar Energy Engineering, Vol. 138, Issue 2, 2014
[6] O. Ojo, "Analysis of current source induction motor drive fed from photovoltaic energy source" IEEE Transactions on Energy Conversion, Vol. 6, No. 1, March 1991, pp 99-106
[7] M. Barlaud, B. de Fornel, M. Gauvrit, J.P. Requier "Computation of optimal functions for transients of photovoltaic array inverter induction motor generator" IEEE Proceedings, Vol. 133, Pt B, No. 1, January 1996, pp 16-19
[8] Q. Wasynczuk, "Modelling and dynamic performance of line-commutated photovoltaic inverter system" IEEE Transactions on Energy Conversion, Vol. 4, No. 3, September 1989, pp 337-343
[9] Q. Wasynczuk, "Modelling and dynamic performance of a self-commutated photovoltaic inverter system" IEEE Transactions on Energy Conversion, Vol. 4, No. 3, September 1989, pp 322-328
[10] S.R. Bhat, A. Pittet, B.S. Sonde "Performance optimization of induction motor pumping system using photovoltaic energy source" IEEE Transactions on Industry Applications, Vol. 1A-23, November/December 1987, pp 995-1000
[11] W.R. Anis, "Analysis of a three-level bridge inverter for photovoltaic" Solar Cells, Vol. 25, 1988, pp 255-263
[12] S.R. Bowes, "Microprocessor control of PWM inverters" IEE Proceedings, Vol. 128, Pt. B, No. 6, November 1981
[13] N.K. Lujara, "Determination of losses in dc-dc converters based on experimental results" Internal Report, END-402, Rand Afrikaans University, November 1997
[14] N.K. Lujara, "Computer aided modelling of systems for solar powered water pumping by photovoltaics" *D.Ing thesis*, Rand Afrikaans University, January 1999, Ch.4 pp 135
[15] International Rectifier Power Mosfet Data and Application Notes, 233 Kansas St. California 90245, Fourth edition pp 1026